J. Plasma Physics (2001), *vol.* 65, *part* 3, *pp.* 197–212.
DOI: 10.1017/S002237780100109X Printed in the United Kingdom

Stationary waves in a bi-ion plasma transverse to the magnetic field

J. F. McKENZIE,[1,2] K. SAUER[1] and E. DUBININ[1,3]

[1]Max-Planck Institut für Aeronomie, Katlenburg–Lindau, Germany

[2]School of Pure and Applied Physics, University of Natal, Durban, South Africa

[3]Centre d'Etude des Environments Terrestre et Planetaires, Velizy, France

(Received 25 September 2000)

Abstract. We investigate the nature of stationary structures streaming at subfast magnetosonic speeds perpendicular to the magnetic field in a bi-ion plasma consisting of protons and a heavy ion species in which the magnetic field is frozen into the electrons, whose inertia may be neglected. The study is based on the properties of the structure equation for the system, which is derived from the equations of motion and the Maxwell equations, and therefore reflects the coupling between the two ion fluids and the electrons through the Lorentz forces and charge neutrality. The basic features of the structure equation are elucidated by making use of conservation of total momentum and charge neutrality, which provide relations between the ion speeds in the unperturbed flow direction and the electron speed. This combination of relations, which we call the momentum hodograph of the system, reveals the structure of the flow and the magnetic field in a solitary-type pulse. In particular, we find that in the initial portion of a compressive soliton, heavy ions run ahead of the electrons and the protons lag between them until a point is reached where they all once more attain the same speed, after which the protons run ahead and are accelerated whereas the heavies now lag behind the continuously decelerating electrons. The second half of the wave is a mirror image of the first portion. The strength of the compression (the amplitude of the wave) is determined from the momentum hodograph, and depends upon the initial Mach number, abundance ratio of heavies to protons and the mass ratio. The analysis is relevant to subfast flows of mass-loaded plasmas and pile-up boundaries, which appear near comets and non-magnetic planets.

1. Introduction

In many space plasma phenomena, heavy ions are present in abundances that are not negligible relative to protons. Cometary plasma is generally a mixture of the solar wind, which is dominated by the protons, and cometary matter, which becomes ionized by photoionization and charge-exchange processes. Multi-ion plasmas also exist near non-magnetized planets, where the solar wind has direct access to ionospheric and atmospheric planetary shells.

The multicomponent nature of space plasmas gives rise to interesting new effects due to the coupling brought about the Lorentz forces and the quasi-charge-neutrality constraint. For example, the fact that alpha particles are observed to

flow faster than protons in the solar wind reveals specific features of stationary flows in multi-ion plasmas. McKenzie et al. (1993) and McKenzie (1994) have shown that a differential streaming between the protons and the alphas can lead to low-frequency compressional instabilities. In addition, these studies provide a generalization of the idea of stationary waves and critical points in multi-ion plasmas that may be applied to the flow of minor ions in the solar wind (Czechowsky et al. 1998). The problem of critical points also appears in problems associated with the origin of unexpected plasma boundaries found near comets and Mars (Sauer et al. 1994). At some of these boundaries, the proton number density drops while the density of the heavies either increases or remains essentially constant. This kind of transition is accompanied by pile-up of the magnetic field (Sauer and Dubinin 2000).

Baumgärtel and Sauer (1992) and Sauer et al. (1992) have considered the simple case of steady flow of a proton–electron plasma around a very heavy (immobile) ion cloud. In the case of field-aligned flow, there is a critical peak density for the heavies above which a steady-state solution for plasma flow does not exist. In the case of a transverse magnetic field, the flow picture becomes more complicated because of the appearance of the Lorentz force, and the singularity point occurs when a critical column density is achieved. In the general case of mobile heavies, the motion of all three populations (electrons, protons and heavies) becomes strongly coupled. Motivated by the problem of stationary flows in multi-ion plasmas and, as is believed, by the related problem of discontinuity-like boundaries observed near comets and unmagnetized planets, which are not predicted in the single-ion MHD approach, we examine the properties of nonlinear stationary structures in a bi-ion plasma.

The addition of new ion species modifies the characteristics of plasma waves (Smith and Brice 1964; Mann et al. 1997) by producing a new cutoff frequency and the appearance of a new mode. Observations near comets provide not only examples of 'random' wave phenomena associated with multi-ion plasmas but also well-isolated, coherent events (Tsurutani et al. 1987; Russell et al. 1987; Glassmeier et al. 1993). Certain types of nonlinear waves and solitons were theoretically studied by Verheest (1990) and Hackenberg et al. (1998). Observations of strongly nonlinear waves near comets Giacobini–Zinner and Grigg–Skjellerup led Verheest (1990) to study soliton solutions for Alfvén waves propagating parallel to the magnetic field when ion species stream differentially. In this case, the structure equation is of the derivative nonlinear Schrödinger type. The relative streaming increases the width and decreases the amplitude of the solitons. Hackenberg et al. (1998) have obtained fast and slow soliton waves with compression and rarefaction characterized by correlation and anticorrelation between the magnetic field and plasma density in the case of oblique propagation.

Here we consider soliton-like solutions in a bi-ion plasma for the simple case where the magnetic field is transverse to the flow (see also Sauer et al. 2000). The properties of compression and rarefaction solutions may be deduced from the momentum hodograph (see below).

The layout of the paper is as follows. The governing equations are presented in Sec. 2. These are the fluid equations for each ion species, which are coupled together through the Lorentz force and the Maxwell equations. The magnetic field is frozen into the electrons, so that Hall-current effects are automatically included and differential streaming between the ion species automatically arises. In Sec. 3, we consider the special case of a steady flow perpendicular to the magnetic field,

and derive the structure equation for one-dimensional stationary nonlinear waves (e.g. solitons). The idea of the momentum hodograph of the system is introduced in Sec. 4 by using the combination of total momentum conservation and charge neutrality, which provides algebraic relations between the ion velocities and the electron velocity in the direction of the unperturbed flow at any point in the structure. This section shows how the hodograph plane proves to be a useful tool in understanding the flow patterns and the magnetic field of the wave. The results are summarized in Sec. 5, in which we discuss their relevance to pile-up boundaries.

2. Governing equations

The equations of continuity and motion for each ion species with density n_i, velocity $\mathbf{u}_i$, pressure p_i, mass m_i and charge eZ_i are

$$\frac{\partial n_i}{\partial t} + \boldsymbol{\nabla} \cdot (n_i \mathbf{u}_i) = 0 \tag{1}$$

$$m_i n_i \frac{D_i \mathbf{u}_i}{Dt} = eZ_i n_i (\mathbf{E} + \mathbf{u}_i \times \mathbf{B}) - \boldsymbol{\nabla} p_i \tag{2}$$

$$\frac{D_i}{D_t} \equiv \frac{\partial}{\partial t} + \mathbf{u}_i \cdot \boldsymbol{\nabla}, \tag{3}$$

where $\mathbf{B}$ and $\mathbf{E}$ are the magnetic and electric fields respectively. The latter may be eliminated from the system through Ohm's law,

$$\mathbf{E} = -\mathbf{u}_e \times \mathbf{B} - \frac{\boldsymbol{\nabla} p_e}{e n_e}, \tag{4}$$

which follows from the electron equation of motion, in which electron inertia is neglected. The magnetic field evolves according to Faraday's law, which, on using (3) for $\mathbf{E}$ and assuming a functional relationship between p_e and n_e, may be written in the form

$$\frac{D_e \mathbf{B}}{Dt} = \mathbf{B} \cdot \boldsymbol{\nabla} \mathbf{u}_e - \mathbf{B} \boldsymbol{\nabla} \cdot \mathbf{u}_e, \tag{5}$$

$$\frac{D_e}{Dt} \equiv \frac{\partial}{\partial t} + \mathbf{u}_e \cdot \boldsymbol{\nabla}. \tag{6}$$

The magnetic field is frozen into the electron fluid. The remaining Maxwell equation, Ampère's law, is

$$\frac{1}{\mu_0} \boldsymbol{\nabla} \times \mathbf{B} = \mathbf{J} + \epsilon_0 \frac{\partial \mathbf{E}}{\partial t}, \tag{7}$$

where, for the moment, the displacement current is retained. The current $\mathbf{J}$ and charge density σ are given by

$$\mathbf{J} = \sum_i eZ_i n_i \mathbf{u}_i - e n_e \mathbf{u}_e, \tag{8a}$$

$$\sigma = \sum_i eZ_i n_i - n_e. \tag{8b}$$

These quantities are related through continuity by

$$\boldsymbol{\nabla} \cdot \mathbf{J} + \frac{\partial \sigma}{\partial t} = 0, \tag{9}$$

https://doi.org/10.1017/S002237780100109X Published online by Cambridge University Press

so that the Poisson equation

$$\epsilon_0 \boldsymbol{\nabla} \cdot \mathbf{E} = \sigma \tag{10}$$

follows as a consequence of the continuity and Faraday equations. The total momentum equation for the system is obtained by adding (2) together with the electron equation of motion to yield

$$\sum_i m_i n_i \frac{D_i \mathbf{u}_i}{Dt} = -\boldsymbol{\nabla}\left(\sum_i p_i + p_e\right) + \epsilon_0 \mathbf{E}\boldsymbol{\nabla}\cdot\mathbf{E} + \mathbf{J}\times\mathbf{B}. \tag{11a}$$

If we impose the quasi-charge-neutrality condition $\sigma \approx 0$, the second term on the right-hand side of (11a) may be neglected, and also, to be consistent, we neglect the displacement current in (7) and expand $\mathbf{J}\times\mathbf{B}$ to obtain total momentum conservation in the form

$$\sum_i m_i n_i \frac{D_i \mathbf{u}_i}{Dt} + \boldsymbol{\nabla}\left(\sum_i p_i + p_e + \frac{B^2}{2\mu_0}\right) - \mathbf{B}\cdot\boldsymbol{\nabla}\mathbf{B} = 0. \tag{11b}$$

In this form, the electric field stresses and the rate of change of momentum associated with the Poynting vector are relativistically small compared with the magnetic field stress, and hence may be neglected. This is the standard MHD approximation, except that $\mathbf{B}$ is frozen into the electrons, and therefore Hall-current effects are automatically included in the system as a whole.

3. Stationary structures with variations perpendicular to the magnetic field in a bi-ion system

Here we consider the special case of $\mathbf{B} = (0, 0, B)$, $\mathbf{u}_i = (u_{ix}, u_{iy}, 0)$, $D_i/Dt = u_i\, d/dx$; that is, the ion flows are perpendicular to the magnetic field, variations are only in the x-direction and the system is stationary ($\partial/\partial t = 0$). The continuity equation becomes

$$n_i u_{ix} = j_i, \quad \text{a constant} \tag{12a}$$

or

$$m_i n_i u_{ix} = M_i, \quad \text{a constant}. \tag{12b}$$

The total-momentum equation integrates immediately to yield

$$\sum_i (M_i u_{ix} + p_i) + p_e + \frac{B^2}{2\mu_0} = Mx, \quad \text{a constant}, \tag{13a}$$

$$\sum_i M_i u_{iy} = M_y, \quad \text{a constant}, \tag{13b}$$

where M_x and M_y are the x and y components of the conserved momentum. Faraday's law reduces to

$$u_{ex} B = E_y, \quad \text{a constant}. \tag{14}$$

In an adiabatic systems, we have

$$\frac{p_i}{n_i^{\gamma_i}} = \text{const} \quad \text{or} \quad p_i u_{ix}^{\gamma_i} = \text{const}, \tag{15a}$$

$$\frac{p_e}{n_e^{\gamma_e}} = \text{const} \quad \text{or} \quad p_e u_{ex}^{\gamma_e} = \text{const}. \tag{15b}$$

https://doi.org/10.1017/S002237780100109X Published online by Cambridge University Press

Equations (12)–(15) represent the important conserved quantities of mass, momentum, the y component of the electric field and entropy. In addition, the charge-neutrality condition is

$$n_e = \sum_i Z_i n_i. \tag{16}$$

The x and y components of the equations of motion (2) may be written as

$$\frac{1}{\Omega_i}\frac{D_i u_{ix}}{Dt} = u_{iy} - u_{ey} - \frac{1}{\Omega_i}\left(\frac{\nabla_x p_i}{m_i n_i} + \frac{\nabla_x p_e}{m_e n_e}\right), \tag{17a}$$

$$\frac{1}{\Omega_i}\frac{D_i u_{iy}}{Dt} = u_{ex} - u_{ix}, \tag{17b}$$

in which Ω_i, is the ion gyrofrequency,

$$\Omega_i = Z_i eB/m_i. \tag{17c}$$

In a bi-ion plasma, $i = p$ (protons) or $i = h$ (heavy ions), subtracting the x components of the equations of motion from each other eliminates the transverse electron velocity u_{ey} and the electron pressure-gradient term to yield

$$\frac{1}{\Omega_p}\left(1 - \frac{u_{px}^2}{c_p^2}\right)\frac{D_p u_{px}}{Dt} - \frac{1}{\Omega_h}\left(1 - \frac{u_{hx}^2}{c_h^2}\right)\frac{D_h u_{hx}}{Dt} = \begin{cases} u_{hy}(1 + M_h/M_p), \\ u_{py}(1 + M_p/M_h), \end{cases} \tag{18}$$

in which transverse momentum with $M_y = 0$ has been used to eliminate either u_{py} or u_{hy} on the right-hand side, and the adiabatic relations (15) eliminate p_i in favour of u_{ix}, where we have introduced the ion sound speed c_i,

$$c_i^2 = \frac{\gamma_i p_i}{m_i n_i} \propto u_{ix}^{-(\gamma_i - 1)}. \tag{19}$$

The operation of D_h/Dt on (18) and the use of (17b) with $i = h$ eliminates u_{iy} in favour of $u_{ex} - u_{hx}$ to yield

$$\frac{D_h}{Dt}\left[\frac{1}{\Omega_p}\left(1 - \frac{u_{px}^2}{c_p^2}\right)\frac{D_p u_{px}}{Dt} - \frac{1}{\Omega_h}\left(1 - \frac{u_{hx}^2}{c_h^2}\right)\frac{D_h u_{hx}}{Dt}\right] = -\frac{j_h}{j_p}\left(1 + \frac{M_p}{M_h}\right)\Omega_p(u_{ex} - u_{hx}). \tag{20}$$

Clearly an alternative equation may be obtained with the operation of D_p/Dt on the left-hand side of (18), with the result that an equivalent right-hand side involving $\Omega_h(u_{ex} - u_{px})$ would appear. Equation (20), a second-order differential equation, determines the structure of the transition. It is in fact a second-order differential equation for u_{ex}. This is the natural (physical as well as mathematical) independent variable of the system in the sense not only that a deceleration in u_{ex} measures magnetic and electron pressure compressions but also because u_{hx} and u_{px} can be expressed in terms of u_{ex} by using conservation of the x component of momentum and the charge-neutrality condition, as we shall see subsequently.

4. The momentum hodograph and the structure equation

The charge-neutrality condition (16) together with the fact that $J_x = 0$ provides the following relation between the x components of the electron, proton and heavy-ion

https://doi.org/10.1017/S002237780100109X Published online by Cambridge University Press

velocities:

$$u_{px} = u_{ex} + \frac{j_h}{j_p} u_{px} \left(\frac{u_{ex}}{u_{hx}} - 1 \right). \tag{21}$$

This simple relation tells us that if the heavy ions lag behind the electrons ($u_{hx} < u_{ex}$), the protons run ahead of the electrons ($u_{px} > u_{ex}$), and vice versa. Moreover, (21) combined with conservation of x momentum (13a) constitute two coupled algebraic equations for the variables u_{px}, u_{hx} and u_{ex}. In principle, these may be solved to give u_{px} and u_{hx} as functions of u_{ex} (and the parameters m_h/m_p, the mass ratio, j_h/j_p, the flux number density ratio, and the fast Mach number). The structure equation (20) may be written in the form

$$\frac{1}{\Omega_p} \frac{d}{dx} \left\{ \left[\left(1 - \frac{c_p^2}{u_{px}^2} \right) \left(1 + \frac{j_h u_{px}}{j_p u_{hx}} \right) u_{hx} \frac{du_{px}}{du_{ex}} + \frac{u_{hx}}{M_p} \frac{d}{du_{ex}} \left(p_e + \frac{B^2}{2\mu_0} \right) \right] \frac{1}{\Omega_p} \frac{du_{ex}}{dx} \right\}$$
$$= - \left(\frac{j_h}{j_p} \right)^2 \left(1 + \frac{M_p}{M_h} \right) \left(\frac{u_{ex}}{u_{hx}} - 1 \right), \tag{22}$$

in which

$$\frac{du_{px}}{du_{ex}} = \frac{1 + \dfrac{j_h u_{px}}{j_p u_{hx}} + \dfrac{m_p}{m_h} \dfrac{u_{ex} u_{px}}{u_{hx}^2} \dfrac{1}{M_p} \dfrac{dP}{du_{ex}} \left(1 - \dfrac{c_h^2}{u_{hx}^2} \right)}{1 + \dfrac{j_h}{j_p} \left(\dfrac{u_{ex}}{u_{hx}} - 1 \right) - \dfrac{m_p}{m_h} \dfrac{u_{ex} u_{px}}{u_{hx}^2} \dfrac{1 - c_p^2/u_{px}^2}{1 - c_h^2/u_{hx}^2}}, \tag{23a}$$

$$\frac{1}{M_p} \frac{dP}{du_{ex}} \equiv \frac{1}{M_p} \frac{d}{du_{ex}} \left(p_e + \frac{B^2}{2\mu_0} \right) = - \left[\frac{1}{M_A^2} \left(\frac{u_0}{u_{ex}} \right)^3 + \frac{1}{M_e^2} \left(\frac{u_0}{u_{ex}} \right)^{\gamma e + 1} \right] \tag{23b}$$

$$M_A^2 = \frac{u_0^2}{V_A^2}, \qquad M_e^2 = \frac{u_0^2}{V_e^2}, \qquad V_A^2 = \frac{B_0^2}{\mu_0 m_p n_{p0}}, \qquad V_e^2 = \frac{\gamma p_{e0}}{m_p n_{p0}}, \tag{23c}$$

where (23a) follows from differentiating x momentum and charge neutrality with respect to u_{ex} The subscript 0 refers to plasma values of the impinging flow at infinity ($x = -\infty$). Equation (22) is a second-order nonlinear differential equation for u_{ex} in which u_{px} and u_{hx} are functions of u_{ex} through the solution of the momentum equation and the charge-neutrality condition. We shall call these relations the momentum hodograph for the system. It proves to be a useful tool in understanding the behaviour of the solutions of (23), all of which must lie on the phase plane of the momentum hodograph. Thus, if we know how u_{px} and u_{hx} vary with u_{ex}, the qualitative structure of the transition of a stationary wave is readily understood. The natural length scale in the structure equation is the Larmor radius of the protons enhanced by the abundance ratio, i.e. $(u_0/\Omega_{p0}) n_p/n_h$.

However, before proceeding to a discussion of the solutions of the full nonlinear structure equation, we note that the linearized version of (23) in a massive-ion limit in the neighbourhood of the initial state yields solutions of the form $\exp(\kappa x)$, where

https://doi.org/10.1017/S002237780100109X Published online by Cambridge University Press

κ is given by

$$\kappa^2 = \frac{\dfrac{\Omega_p^2}{u_0^2}\left(\dfrac{n_h}{n_p}\right)_0^2\left(1+\dfrac{M_p}{M_h}\right)}{\dfrac{V_A^2+V_e^2}{u_0^2} - \left(1-\dfrac{c_p^2}{u_0^2}\right)\left[1+\left(\dfrac{n_h}{n_p}\right)_0\right]\left(\dfrac{du_p}{du_e}\right)_0}. \tag{24a}$$

This is the stationary-wave dispersion equation for the system, and requires the flow to be 'subfast' ($u_0 < (V_A^2+V_e^2)^{1/2}/(1+n_h/n_p)_0$) to ensure exponential behaviour ($\kappa^2 > 0$), which in turn permits the build up of a nonlinear structure. The dispersion equation for propagating waves ($\propto \exp(i\omega t - ikx)$) follows from (24a) using the transformations $u_0 \to \omega/k$ and $\kappa \to ik$; and for the case of massive ($m_p/m_h \ll 1$) cold ions and protons ($c_p = c_h = 0$), we obtain the simple and clear relation

$$\omega^2 = \frac{(V_A^2+V_e^2)k^2 + \Omega_p^2(n_h/n_p)_0^2}{[1+(n_h/n_p)_0]^2}. \tag{24b}$$

This shows the existence of a cut-off frequency

$$\omega_c = \frac{\Omega_p(n_h/n_p)_0}{1+(n_h/n_p)_0}, \tag{24c}$$

below which the waves are evanescent and above which the wave propagates with the fast-mode speed reduced by $1+(n_h/n_p)$, at long wavelengths. This tells us that near the endpoints of the wave, the structure equation reduces to the Klein–Gordon type. At very low frequencies and long wavelengths, the exact dispersion equation shows there is a new ion-cyclotron-type mode associated with the heavies, displaying a resonance, and whose speed at the lowest frequencies is essentially the Alfvén speed based on the total mass density (Smith and Brice 1964; Sauer et al. 1990). We should therefore find that stationary waves of evanescent type would require higher Alfvén speeds than this value in the very low-frequency limit.

To illustrate the usefulness of the momentum-hodograph view, let us consider the simplest (algebraically) case of cold ions and electrons, so that only the magnetic pressure is available to balance changes in the momentum of the protons and heavies. Eliminating u_{px} from the cold version of x-momentum conservation using (21) gives a quadratic equation in u_{hx}, whose solutions, in normalized form, may be written

$$u_h - 1 = \frac{-b \pm \sqrt{b^2-4ac}}{2a}, \tag{25}$$

where

$$a \equiv \frac{m_h n_h}{n_p m_p}u_\infty, \tag{26a}$$

$$b \equiv \frac{m_h n_h}{m_p n_p}(u_\infty - u_e) + \frac{u_e n_p}{n_h} - u_\infty - \frac{u_\infty}{2M_A^2}(1-u_e^{-2}), \tag{26b}$$

$$c \equiv -\left[\frac{(u_\infty - u_e)(1-u_e^{-2})}{2M_A^2} - u_\infty(u_e-1)\right], \tag{26c}$$

$$u_\infty = 1 + \frac{j_p}{j_h} = 1 + \frac{n_p}{n_h} \tag{26d}$$

https://doi.org/10.1017/S002237780100109X Published online by Cambridge University Press

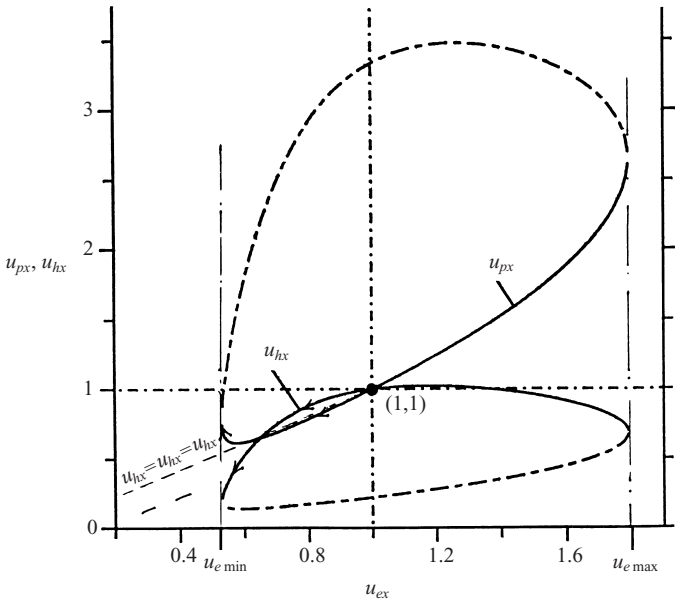

Figure 1. The loci of u_{px} and u_{hx} for a set of parameters $M_A = 0.7$, $n_h/n_p = 0.2$ and $m_h/m_p = 15$ defining the initial state. All solutions of the structure equation lie on these loci, which we refer to as the momentum hodograph. Compressive solitons evolve along the curves to the left of the initial point ($u_{ex} < 1$), whereas rarefaction solitons (if they exist) evolve along the curves to the right ($u_{ex} > 1$). The strength of the soliton is defined by $u_{e\,\min}$ (compression) or $u_{e\,\max}$ (rarefaction). The broken curves are inaccessible from the initial point except through discontinuities.

$$u_h \equiv \frac{u_{hx}}{u_0}, \qquad u_e \equiv \frac{u_{ex}}{u_0}, \qquad u_p \equiv \frac{u_{px}}{u_0}, \tag{26e}$$

in which u_0 is the incoming speed and n_h/n_p is the heavy abundance relative to the protons. Thus, with (25) determining u_h as a function of u_e (for given parameters m_h/m_p, n_h/n_p and the fast Mach number M_A), the charge-neutrality relation (21) provides u_p as a function of u_e, which in normalized form becomes

$$u_p = \frac{(n_p/n_h)u_e}{u_\infty - u_e/u_h}. \tag{27}$$

Equations (26 and 27) are the explicit form of the momentum hodograph in the case of a cold plasma. The maximum compression (or rarefaction) that can be attained in such a wave is given by value of u_e that makes $b^2 - 4ac = 0$ in (24a). Figure 1 shows the locii of u_p and u_h as functions of u_e. Initially (at the point (1,1)), the protons and heavies are decelerated along with the electrons, with the heavies running ahead of and the protons lagging behind the electrons. Near the end of the compression ($u_e = u_{e\,\min}$), the protons then run ahead of the electrons and the heavies lag behind. The structure is completed as a mirror image, with the protons and heavies evolving back along the loci to return to the initial state.

An exact numerical solution of the structure equation (22) is shown in Fig. 2, which displays all the features revealed by the momentum hodograph. It should be noted that the change in sign of the y component of the Lorentz force is also evident in the intersection between the hodograph curves and the line $u_p = u_h = u_e$, where we see that where $u_p > u_e$ and $u_h < u_e$ near the centre of the wave, the protons and

https://doi.org/10.1017/S002237780100109X Published online by Cambridge University Press

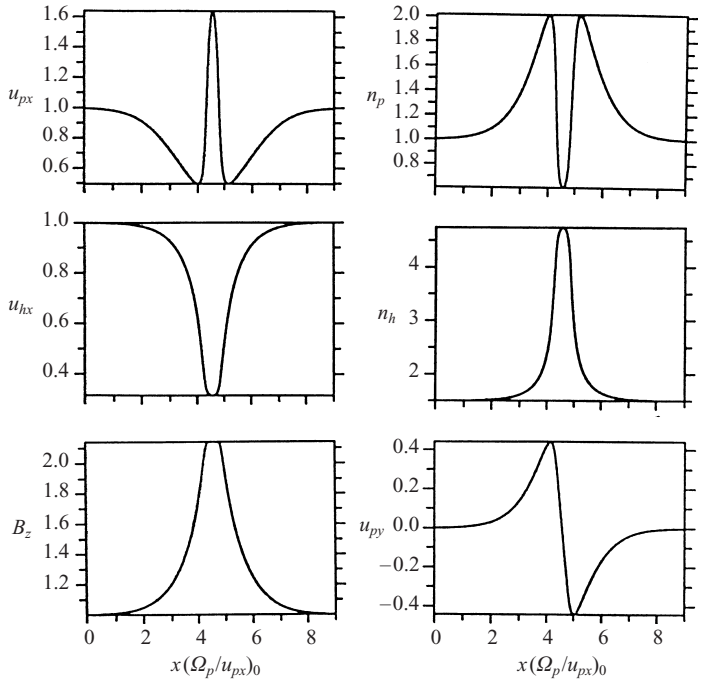

Figure 2. The structure of a compressive soliton for $m_h/m_p = 15$, $n_h/n_p = 1.5$ and $M_A = 0.3$. Note that near the centre of the wave, the protons are depleted because of their rapid acceleration there. The maximum compression in B is about 2.1, corresponding to $u_{e\,\min} = 0.48$.

heavies are deflected in opposite directions, with the mirror image of this solution pertaining after the centre of the wave.

Figure 3(a) shows $u_{e\,\min}$ (from $b^2 = 4ac$), which determines the maximum strength of the compression ($B_z \propto 1/u_e$) as a function of the Alfvén Mach number M_A for given $(n_h/n_p)_0$ and m_h/m_p. As M_A increases, $u_{e\,\min}$ ($B_{\max}$) decreases (increases). In the limit $u_e \to 1$, $M_A \to 0$, the following provides a good approximation to the maximum compression: and

$$u_{e\,\min} \approx 1 - \frac{M_A^2}{u_\infty}\left(1 + \frac{m_h}{m_p} - 2\sqrt{\frac{m_h}{m_p}}\right). \tag{28a}$$

In a plasma dominated by the heavies, the maximum compression increases, and is given approximately by

$$u_{e\,\min} \approx \frac{1}{\sqrt{2}M_A}\frac{1}{\sqrt{1 + \dfrac{m_h n_h}{m_p n_p}}}. \tag{28b}$$

The compression is also enhanced by increasing the abundance of the heavy ions. This is clearly seen in Fig. 3(b), which shows $u_{e\,\min}$ as a function of the number-density ratio n_h/n_p for given values of M_A and the mass ratio m_h/m_p. Examples of the momentum hodograph are displayed in Fig. 4, which, for a given heavy-to-proton mass ratio, shows the effect of varying the abundance ratio n_h/n_p and the fast Mach number M_A on the relations between u_p, u_h and u_e. All display the interesting feature that as the solution evolves from the initial point ($u_p = u_h = u_e = 1$

https://doi.org/10.1017/S002237780100109X Published online by Cambridge University Press

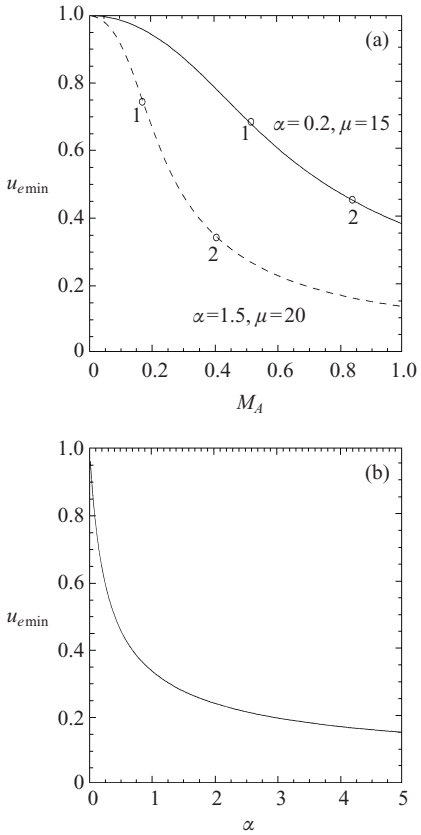

Figure 3. (a) The inverse maximum compression $u_{e\,\min}$ as a function of M_A for different mass and density ratios. Solitons are permitted only between the points 1 and 2 in order to satisfy the evanescent criterion. (b) $u_{e\,\min}$ as a function of the density ratio $\alpha = n_h/n_p$ for a given $M_A = 0.5$ and $\mu = m_h/m_p = 20$.

at $x = -\infty$), the heavies at first run ahead of the electrons ($u_h > u_e$) and the protons lag behind ($u_p < u_e$), until a point is reached where all fluids are decelerated to the same speed ($u_p = u_h = u_e$), after which the protons run ahead of the electrons and accelerate while the heavies now lag behind the electrons, both of which continue to decelerate until the electrons reach a critical speed below which there are no real solutions for u_p and u_h corresponding to the maximum compression of the magnetic field and the electron density. The structure then evolves back up the $(u_{p,h}, u_e)$ curves to return to the initial values (now at $x = +\infty$); that is, the second half is a mirror image of the first half of the solution. The top panel on the left displays the interesting feature that once the protons are accelerated and run ahead of the electrons, they can attain speeds in excess of their entry speed (i.e. $u_p > 1$), with the result that their initial compression is followed by an expansion near the centre of the wave.

Figure 5 shows the speeds of the protons and the heavy ions at the critical point of maximum deceleration of the electrons as a function of the initial flow speed. The interesting feature is that the protons gain the maximum momentum at low Mach numbers. If we use the analytical expression (28a) for u_e and take $M_A \to 0$,

https://doi.org/10.1017/S002237780100109X Published online by Cambridge University Press

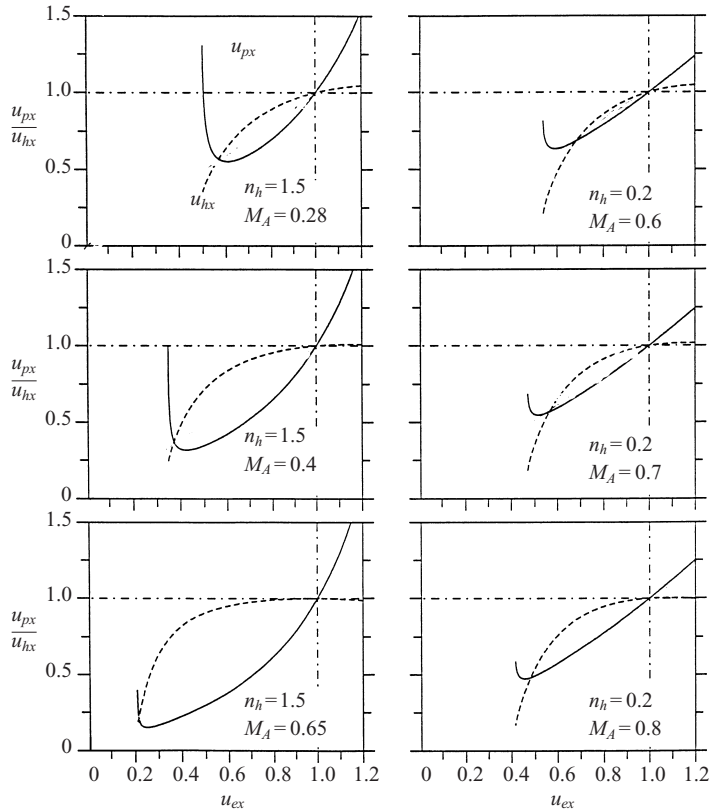

Figure 4. Examples of the compressive portion of the momentum hodograph for a variety of different parameters.

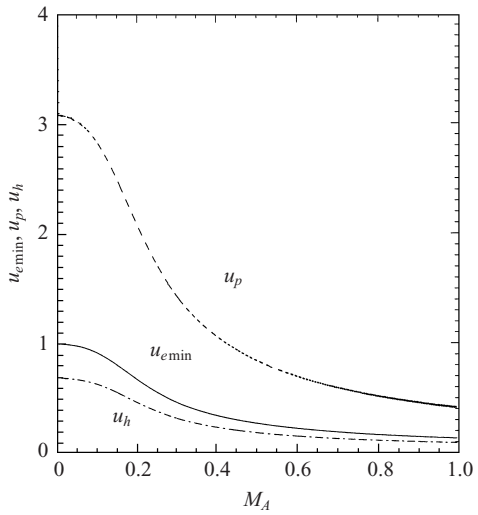

Figure 5. The limiting values of u_p and u_h associated with $u_{e\,\min}$ as functions of the Mach number M_A for $\alpha = n_h/n_p = 1.5$ and $\mu = m_h/m_p = 20$. Note the jumps in u_p and u_h at $M_A = 0$, where $u_{e\,\min} = 1$.

https://doi.org/10.1017/S002237780100109X Published online by Cambridge University Press

we find from (25) and (27) that u_h and u_p are given by

$$u_h = \frac{\dfrac{n_h}{n_p} + \sqrt{\dfrac{m_p}{m_h}}}{1 + \dfrac{n_h}{n_p}}, \tag{29a}$$

$$u_p = \sqrt{\frac{m_h}{m_p}}\,\frac{1 + \dfrac{n_p}{n_h}\sqrt{\dfrac{m_p}{m_h}}}{1 + \dfrac{n_p}{n_h}}. \tag{29b}$$

This is noteworthy in that although $u_e \to 1$ u_h jumps down (to about 0.69 for the case shown in Fig. 5) and u_p jumps up (to about 3.05) to conserve the finite jump in normalized magnetic pressure given by $m_h/m_p + 1 - 2\sqrt{m_h/m_p}$, which follows from (28a). Figure 6 shows the momentum hodograph as this interesting limit is approached. The behaviour of the various quantities $u_{ex}(B)$, u_{px} and u_{hx} near the point of maximum compression (i.e. the centre of the soliton) follows from approximate solutions of the structure equation (23). With $u_{e\,\min}$ as the value of u_e that makes $b^2 = 4ac$ in (25a), it follows that

$$u_e \approx u_{e\,\min} + k_e x^4, \tag{30a}$$

$$u_h \approx u_{h\,\min} + k_h x^2, \tag{30b}$$

$$u_p \approx u_{h\,\min} - k_p x^2, \tag{30c}$$

where the constant k_e follows from the structure equation and relates to values in the neighbourhood of $u_{e\,\min}$, and k_h and k_p follow from the momentum hodograph. The interesting feature here is that u_e approaches its minimum value in a much 'flatter' way than u_h approaches its minimum and u_p approaches its maximum. This feature is reflected in the momentum hodograph, which shows that as the centre of the wave is approached, changes in momentum are taken up by an acceleration of the protons and a deceleration in the heavies because the magnetic pressure has 'run out of steam'.

In principle, the properties of rarefaction stationary waves can be deduced from inspecting the momentum hodograph in the region $u_e > 1 (B < 1)$. For example, Fig. 1 shows that the protons run ahead of the electrons and are continuously accelerated up to a limiting value (corresponding to where u_e reaches $u_{e\,\max}$). On the other hand, the heavies lag behind ponderously and are decelerated to their limiting value. In Fig. 7, the inverse maximum expansion of B measured by $u_{e\,\max}$ is plotted as a function of the Alfvén Mach number along with the corresponding limiting values of u_p and u_h. For small M_A and massive ions, $u_{e\,\max}$ is approximated by

$$u_{e\,\max} \approx 2\frac{n_p m_p}{n_h m_h}\left(\sqrt{\frac{u_\infty}{2M_A^2}} - \sqrt{\frac{m_h}{m_p}}\right)^2. \tag{31}$$

However, an analysis of the structure equation (22) shows that it has a critical point where the square bracket on the left hand is zero at some value $u_e = u_c$, say, near which the solutions may be approximated by

$$\frac{(u_e - u_c)^2}{2} + k\left[\left(\frac{u_e}{u_h}\right)_c - 1\right]\frac{x^2}{2} = c_1 x + c_2, \tag{32a}$$

https://doi.org/10.1017/S002237780100109X Published online by Cambridge University Press

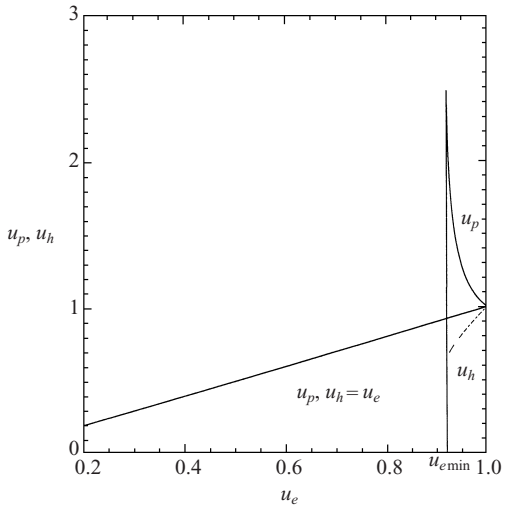

Figure 6. The momentum hodograph for small $M_A = 0.1$, $d = n_h/n_p = 1.5$ and $\mu = m_h/m_p = 20$, showing the 'rapid' acceleration of $u_p \to 3$ and deceleration of $u_h \to 0.7$.

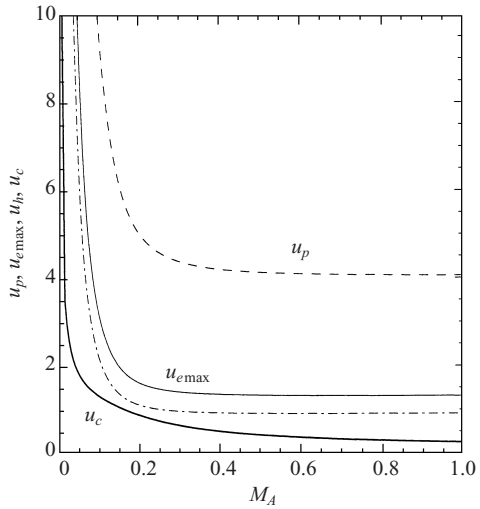

Figure 7. The maximum value $u_{e\,\max}$ (inverse expansion) and the critical velocity u_c for a rarefaction wave as functions of M_A for $\alpha = n_h/n_p = 1.5$ and $\mu = m_h/m_p = 20$.

$$k = \left(\frac{j_h}{j_p}\right)^2 \left(1 + \frac{M_p}{M_h}\right) \Omega_{pc}^2 \frac{u_c}{3} > 0, \tag{32b}$$

where c_1 and c_2 are constants of integration. Since $k > 0$ and $u_e/u_h > 1$, the integral curves are parabolas. Since $u_c < u_{e\,\max}$ (see Fig. 7), this critical point is reached before the expansion is completed, yielding multivalued solutions. Therefore stationary rarefaction solitons cannot exist in this configuration.

Although we have only studied the cold case in detail, the inclusion of electron pressure will not change the qualitative structure of the compression waves, since $p_e \propto u_e^{-\gamma e}$ and therefore the Alfvén Mach number will be replaced by a fast Mach number as indicated in (23b, c). However, the inclusion of proton and heavy pres-

https://doi.org/10.1017/S002237780100109X Published online by Cambridge University Press

sures may effect the structure significantly at low speeds, since critical points are embedded in (20) and (22), and exchanges in momentum between the dynamic pressure and ion pressures may become more important than magnetic and electron pressure changes.

5. Summary

The flow pattern of stationary waves propagating at subfast speeds perpendicular to the magnetic field in a bi-ion plasma is elucidated by making use of the 'momentum hodograph' of the system. The combination of momentum conservation, charge neutrality and zero current in the direction of propagation provides the locii of u_{px} and u_{hx} as functions of u_{ex} on which all solutions of the structure equation must lie. Thus this phase-plane picture (see e.g. Fig. 1) immediately reveals the flow patterns of the ions and electrons, with the latter measuring the magnetic compression or rarefaction through the frozen-field condition. In a compressive wave, the heavy ions initially run ahead of the electrons while the protons lag behind them, until a point is reached where all species attain the same speed, after which the protons run ahead and the heavies lag behind, and both attain limiting values determined by the maximum compression at the centre of the wave. The wave is completed as a mirror image, with the protons, heavies and electrons returning along the loci to the initial point. The maximum compression is determined by the incoming Mach number and the mass and density ratios (see e.g. Figs 3 and 5). This relation may be thought of as the soliton analogue of the Rankine–Hugoniot compression ratio for ordinary shocks (although they are completely different types of structure). It appears that stationary rarefaction solitons cannot exist, because the integral curves are parabolas near the critical point, leading to choked flow before the expansion can be completed.

An interesting feature of a compressive soliton in a bi-ion plasma where the heavies are not a minor component is that the behaviour of the protons and the heavies becomes totally different. An initial compression of the proton flow is followed by an expansion with significant decrease of the proton number density, while a compression (deceleration) of the heavies continues. Similar heavy-ion bunches were observed near Mars in the magnetosheath, downstream of the bow shock, where the number density of the planetary ions gradually increases (Dubinin et al. 1996a, 1998). It was found that the magnetosheath plasma was often stratified on alternating layers, with dominance of either the solar-wind protons or the heavy planetary ions. Stratification of a bi-ion plasma on alternating shocklet structures was also observed in two-dimensional MHD simulations (Sauer et al. 1994) and one-dimensional hybrid simulations (Omidi and Winske 1986). These periodic structures are characterized by proton decleration at the centre of heavy-ion bunches, with following reacceleration at their middle and rear side. The observed structures resemble the solitons in a bi-ion plasma (see Fig. 2). The important difference is that in the observations, the plasma flow did not recover during the transition across these structures but instead was steplike decelerated and heated. In solitary-type solutions, we have reversible behaviour of a bi-ion flow. It is not unreasonable that the inclusion of dissipation terms in the governing equations may lead to shock-like solutions similar to collisionless shocks in a proton–electron plasma, which may provide reasonable agreement with the observations. Solitary-wave structures were also clearly observed during the Giotto spacecraft flyby at comet Grigg–Skjellerup.

Strongly modulated electron fluxes were seen after the bow-shock crossing in the cometosheath. The structures consisting of narrow peaks and relatively wide spacing were very coherent (Reme et al. 1993).

Another interesting question to be addressed is what happens if a subfast flow of bi-ion plasma is further decelerated owing to the addition of newly generated heavy ions (mass loading) that become more and more massive. From the structure of a compressive stationary solution (Fig. 2), we can assume that, at a certain point, the heavies reach a critical velocity determined by the Alfvén speed for the heavies, and therefore cannot go through this point without shock formation. Protons that are accelerated near this point should also suffer a jump transition. It is possible in this case that, the one-dimensional treatment employed becomes inadequate to describe this transition. In a three-dimensional situation, one may expect the appearance of a proton cavity bounded by a piled-up magnetic field and a heavy-ion shock. Such a scenario may be realized at comets and non-magnetized planets such as Mars, where a sharp magnetic pile-up boundary accompanied by termination of the solar-wind flow was observed far away from the 'ionopause', where the thermal pressure of cometary (planetary) plasma can balance the pressure of the incoming solar wind (Dubinin et al. 1996b; Sauer et al. 1994; Sauer and Dubinin 2000).

References

Baumgärtel, K. and Sauer, K. 1992 Interaction of magnetized plasma stream with immobile ion cloud. *Ann. Geophys.* **10**, 763.

Czechowski, A., Ratkiewicz, R., McKenzie, J. F. and Axford, W. I. 1998 Heating and acceleration of minor ions in the solar wind. *Astron. Astrophys.* **335**, 303.

Dubinin, E. M., Sauer, K., Lundin, R., Baumgärtel, K. and Bogdanov, A. 1996a Structuring of the transition region of the Martian magnetosphere. *Geophys. Res. Lett.* **23**, 785.

Dubinin, E., Sauer, K., Lundin, R., Norberg, O., Trotignon, J.-G., Schwingenschuh, K., Delva, M. and Riedler, W. 1996b. Plasma characteristics of the boundary layer in the Martian magnetosphere. *J. Geophys. Res.* **101**, 27 061.

Dubinin, E. M., Sauer, K., Baumgärtel, K. and Srivastava, K. 1998 Multiple shocks near Mars. *Earth, Planets and Space* **503**, 279.

Glassmeier, K. H., Motschmann, U., Mazelle, C., Neubauer, F. M., Sauer, K., Fuselier, S., and Acuna, M. H. 1993 Mirror modes and fast magnetoacoustic waves near magnetic pileup boundary of comet P/Halley. *J. Geophys. Res.* **98**, 20 955.

Hackenberg, P., Mann, G. and Marsch, E. 1998 Solitons in multi-ion plasmas. *J. Plasma Phys.* **60**, 845.

McKenzie, J. F. 1994 Interaction between Alfvén waves and a multicomponent plasma with differential streaming. *J. Geophys. Res.* **99**, 4193.

McKenzie, J. F., Marsch, E., Baumgärtel, K. and Sauer, K. 1993 Wave and stability properties of multi-ion plasmas with applications to winds and flows. *Ann. Geophys.* **11**, 341.

Mann, G., Hackenberg, P. and Marsch, E. 1997 Linear mode analysis in multi-ion plasmas. *J. Plasma Phys.* **58**, 205.

Omidi, N. and Winske, D. 1987 A kinetic study of solar wind mass loading and cometary bow shocks. *J. Geophys. Res.* **92**, 13 409.

Reme, H., Mazelle, C., Savaud, J. A., D'Uston, C., Froment, F., Lin, R. P. et al. 1993 Electron plasma environment at comet Grigg–Skjellerup: General observations and comparison with the environment at comet Halley. *J. Geophys. Res.* **98**, 20 965.

Russell, C. T., Riedler, W., Schwingenschuh, K. and Yeroshenko, Ye. 1987 Mirror instability in the magnetosphere of comet Halley. *Geophys. Res. Lett.* **14**, 644.

Sauer, K. and Dubinin, E. 2000 The nature of the Martian 'obstacle boundary'. *Adv. Space Res.* **26**, 1633.

Sauer, K., Motschmann, U. and Roatch, Th. 1990 Plasma boundaries at comet Halley. *Ann. Geophys.* **8**, 243.

Sauer, K., Roatsch, T., Baumgärtel, K. and McKenzie, J. F. 1992 Critical density layer as obstacle at solar wind–exospheric ion interaction. *Geophys. Res. Lett.* **19**, 645.

Sauer, K., Bogdanov, A. and Baumgärtel, K. 1994 Evidence of an ion composition boundary (protonopause) in bi-ion fluid simulations of solar wind mass loading. *Geophys. Res. Lett.* **21**, 2255.

Sauer, K., McKenzie, J. F. and Dubinin, E. 2000 Waves and nonlinear structure in bi-ion plasmas. In: *Waves in Dusty, Solar and Space Plasmas* (ed. F. Verheest, M. Goossens, M. A. Hellberg and R. Bharuthram), p. 327. American Institute of Physics Conference Proceedings Series, Woodhead, NY.

Smith, R. L. and Brice, N. 1964 Propagation in multi-component plasmas. *J. Geophys. Res.* **69**, 5029.

Tsurutani, B. T., Thorne, R. M., Smith, E. J., Gosling, J. T. and Matsumoto, H. 1987 Steepened magnetosonic waves at comet Giacobini–Zinner. *J. Geophys. Res.* **92**, 11 074.

Verheest, F. 1990 Nonlinear parallel Alfvén waves in cometary plasmas. *Icarus* **86**, 273.